

# Neutron matter at zero temperature with auxiliary field diffusion Monte Carlo

A. Sarsa,\* S. Fantoni,<sup>†</sup> and K. E. Schmidt<sup>‡</sup>  
*International School for Advanced Studies, SISSA, and  
INFM DEMOCRITOS National Simulation Center  
Via Beirut I-34014 Trieste, Italy*

F. Pederiva<sup>§</sup>  
*Dipartimento di Fisica dell'Università di Trento, and  
INFM DEMOCRITOS National Simulation Center  
I-38050 Povo, Trento, Italy*  
(Dated: November 3, 2018)

The recently developed auxiliary field diffusion Monte Carlo method is applied to compute the equation of state and the compressibility of neutron matter. By combining diffusion Monte Carlo for the spatial degrees of freedom and auxiliary field Monte Carlo to separate the spin-isospin operators, quantum Monte Carlo can be used to simulate the ground state of many nucleon systems ( $A \lesssim 100$ ). We use a path constraint to control the fermion sign problem. We have made simulations for realistic interactions, which include tensor and spin-orbit two-body potentials as well as three-nucleon forces. The Argonne  $v_8'$  and  $v_6'$  two nucleon potentials plus the Urbana or Illinois three-nucleon potentials have been used in our calculations. We compare with fermion hypernetted chain results. We report results of a Periodic Box-FHNC calculation, which is also used to estimate the finite size corrections to our quantum Monte Carlo simulations. Our AFDMC results for  $v_6$  models of pure neutron matter are in reasonably good agreement with equivalent Correlated Basis Function (CBF) calculations, providing energies per particle which are slightly lower than the CBF ones. However, the inclusion of the spin-orbit force leads to quite different results particularly at relatively high densities. The resulting equation of state from AFDMC calculations is harder than the one from previous Fermi hypernetted chain studies commonly used to determine the neutron star structure.

PACS numbers: 26.60.+c, 21.65.+f, 21.30.Fe, 05.10.Ln

## I. INTRODUCTION

The important role played by N–N correlations on several properties of dense and cold hadronic matter is a well established fact [1]. Less established are quantitative studies performed with realistic nuclear interactions derived from N–N data and the spectra of light nuclei. The strong repulsion at short range accompanied with the strong spin-isospin dependence, make *ab initio* calculations of the nuclear matter equation of state one of the most challenging problems in strongly correlated many-body theory.

A theoretical calculation of the nuclear matter energy per particle, as a function of the number density  $\rho$ , the temperature  $T$  and the neutron–proton asymmetry  $\alpha = (N - Z)/(N + Z)$ , with an uncertainty of less than an MeV has become a fundamental issue. On one hand, one would like to use the observational data from neutron stars and supernovae, as well as from heavy-ion

collisions to get information on the many-body nature of the nucleon interaction. On the other hand, it is of interest to understand the effect of N–N correlations, and particularly of those induced by the tensor force, on the structure and the evolution of compact astrophysical objects [2, 3, 4, 5, 6].

In this paper we limit ourselves to non-relativistic model hamiltonians. Modern two-body potentials [7, 8, 9] fit the Nijmegen N–N data [10] below 350 MeV at a confidence level of  $\chi^2/N_{data} \sim 1$ , and to a large extent give equivalent results for several nuclear and neutron matter properties [11]. However, it has become evident that a two-body potential alone is not sufficient to reproduce the experimental data of nuclei other than the deuteron ( $A = 2$ ). In the last few years, the Urbana–Argonne collaboration has produced three-body force models which, when added to the two-body potential, provide a satisfactory fit to the binding energies and the low-lying states of light nuclei with  $A \leq 10$  [12, 13, 14].

It would be desirable to have microscopic calculations of the equation of state of nuclear matter with an accuracy comparable to that of light nuclei or, at least, on the order of the experimental uncertainties of the equilibrium density,  $\rho_0$ , binding energy per particle at  $\rho_0$  and compressibility. This can be considered as the minimal requirement to attempt the study hadronic matter at densities larger than  $\rho_0$ , and/or with large asymmetries ( $\alpha$  close to 1) in a realistic way. Such calculations have to deal necessarily with potentials which are strongly spin-

\*Electronic address: sarsa@sissa.it; Present address: Departamento de Física Moderna, Universidad de Granada, E-18071 Granada, Spain

<sup>†</sup>Electronic address: fantoni@sissa.it

<sup>‡</sup>Electronic address: kevin.schmidt@asu.edu; Permanent address: Department of Physics and Astronomy, Arizona State University, Tempe, AZ, 85287

<sup>§</sup>Electronic address: pederiva@science.unitn.it

isospin dependent and which include a three-body force.

Most of the microscopic calculations of the nuclear matter equation of state carried out in the last decades have been performed by using perturbation theories based either on ladder diagram summation, like Brueckner or Green's Function theories [11, 15], or Correlated Basis Function theories, based on Fermi hypernetted chain techniques [16, 17, 18]. In spite of the important advances made in recent years in the above theories, the required accuracy for the equation of state has not yet been reached.

Quantum Monte Carlo methods have been very successful in calculating the properties of strongly interacting systems in condensed matter physics. They are substantially exact, apart from statistical errors, finite size effects and the well known sign problem [19] for Fermi systems. They have been recently used to perform quantum simulations of light nuclei [14, 20, 21] with modern nonrelativistic Hamiltonians of the type discussed above. However, the exponential growth in the number of spin-isospin states with the number of nucleons  $A$ , has kept this method from being applied to larger nuclear systems.

Auxiliary field diffusion Monte Carlo [22] (AFDMC) has been especially developed to tackle the problem of computing the binding energy of a relatively large nuclear system at the required accuracy. In this approach the particle coordinates are propagated as in standard diffusion Monte Carlo. Auxiliary fields are introduced to uncouple the spin-dependent interaction between particles by means of a Hubbard–Stratonovich transformation. The particle spins only interact with the auxiliary fields which, when integrated, produce the original interaction. The method consists of calculating the auxiliary field integrations by Monte Carlo sampling and then propagating the spin variables. This propagation results in a rotation of each particle's spinor governed by the sampled values of the auxiliary variables. The result is a sampling of the spin variables which should have less variance than a direct approach where the spins are flipped.

The tensor force couples the spin configurations with the orbital angular momentum so that the wave function becomes complex. The resulting fermion phase problem is handled by applying a path-constraint approximation analogous to the fixed-node approximation. The AFDMC method for the spin–isospin calculations can be viewed as a generalization of the method of Zhang et al. [23, 24] used in condensed matter lattice systems to the spin-isospin states of nucleon systems, while retaining standard diffusion Monte Carlo for the spatial degrees of freedom. The AFDMC method has proved to be efficient in dealing with large nucleon systems interacting via semi-realistic potentials [22, 25, 26] and spin-polarized neutron systems [27].

The aim of this paper is to give a detailed description of the AFDMC method and to report results for the equation of state of pure neutron matter ( $\alpha = 1$ ) with a fully realistic nuclear interaction, at zero temperature. It presents results of AFDMC simulations of 14,

38, 66 and 114 neutrons in a periodic box, interacting via a realistic potential which includes two-body tensor and spin–orbit components, as well as three–body forces. Particular attention is paid to the 14 neutron system, which may serve as a homework problem for different many–body techniques. It is small enough to be handled by traditional quantum Monte Carlo methods [28]. However, it will be shown that the finite size effects of 14 neutron systems are hard to estimate in a realistic way. Actually results obtained with larger systems (66 or 114 neutrons) show that the equation of state of neutron matter cannot be simulated starting from 14 neutron in a box, particularly in the high density region. Finite size effects for the larger systems considered here can be fairly well estimated by the recently developed Periodic Box FHNC (PBFHNC) theory [29]. We have also performed AFDMC calculations of the binding energy of symmetric and asymmetric nuclear matter. A few results obtained with semi-realistic spin-dependent central potentials are presented and discussed.

The plan of the paper is the following. The Hamiltonian used in this work is shown in the next section. In section III the problem of the spin degrees of freedom in quantum monte carlo simulations is discussed. Section IV is devoted to the description of the AFDMC method, including the calculation of the spin–orbit and the three–body terms of the Hamiltonian. A discussion of the finite size effects along with the Periodic box FHNC method is given in Section V. The results for the neutron matter equation of state are presented and discussed in Section VI. The conclusions and perspectives for the present work are in Section VII.

## II. THE HAMILTONIAN

We use a non relativistic Hamiltonian of the form

$$H = T + V_2 + V_3 \\ = -\frac{\hbar^2}{2m} \sum_{j=1,N} \nabla_j^2 + \sum_{j < k} v_{jk} + \sum_{j < k < l} V_{jkl} , \quad (1)$$

containing the kinetic term, where we have used  $\hbar^2/(2m) = 20.73554 \text{ MeV fm}^2$  (which corresponds to the  $n-p$  reduced mass), and two– and three–body potentials. The two–body potential belongs to the Urbana–Argonne  $v_\ell$  type

$$v_\ell = \sum_{j < k} v_{jk} = \sum_{j < k} \sum_{p=1}^\ell v_p(r_{jk}) O^{(p)}(j, k) , \quad (2)$$

where  $j$  and  $k$  label the two nucleons,  $r_{jk}$  is the distance separating the two nucleons, and the spin–isospin dependent operators  $O^p(i, j)$  for  $p = 1, 8$  are given by

$$O^{p=1,8}(j, k) = \left( 1, \vec{\sigma}_j \cdot \vec{\sigma}_k, S_{jk}, \vec{L}_{jk} \cdot \vec{S}_{jk} \right) \otimes (1, \vec{\tau}_j \cdot \vec{\tau}_k) , \quad (3)$$

where  $S_{jk} = 3(\hat{r}_{jk} \cdot \vec{\sigma}_j)(\hat{r}_{jk} \cdot \vec{\sigma}_k) - \vec{\sigma}_j \cdot \vec{\sigma}_k$  is the two-nucleon tensor operator, and  $\vec{L}_{jk}$  and  $\vec{S}_{jk}$  are the relative angular momentum and the total spin, given by

$$\vec{L}_{jk} = \frac{\hbar}{2i}(\vec{r}_j - \vec{r}_k) \times (\vec{\nabla}_j - \vec{\nabla}_k) , \quad (4)$$

$$\vec{S}_{jk} = \frac{\hbar}{2}(\vec{\sigma}_j + \vec{\sigma}_k) . \quad (5)$$

The full Argonne  $v_{18}$  potential consists of  $\ell=18$  components. Besides the 8 components given in Eq.(3), it includes the 6 ( $L^2, L^2 \vec{\sigma}_j \cdot \vec{\sigma}_k, (\vec{L} \cdot \vec{S})^2$ )  $\otimes (1, \vec{r}_j \cdot \vec{r}_k)$  charge independent ones, as well as 4 other charge-symmetry-breaking and charge-dependent terms.

We use a simplified isoscalar version of the  $v_{18}$  potential, the so called  $v'_8$  two-body potential [20]. This potential has been obtained with a new fit to the N-N data, with only the first eight spin-dependent operators in Eq.(3) included. It equals the isoscalar part of  $v_{18}$  in all  $S$  and  $P$  waves as well as in the  $^3D_1$  wave and its coupling to the  $^3S_1$ . It has been used in a number of GFMC calculations in light nuclei [20], as well as FHNC/SOC calculations in nuclear matter [17]; differences with the  $v_{18}$  potential give small contributions and can be safely estimated perturbatively or from FHNC/SOC calculations.

For the sake of completeness, we report here the parameterization of the Argonne  $v'_8$  two-body potential.

$$v_p(r) = \sum_{m=1}^8 A_{p,m} F_m(r) , \quad (6)$$

where odd and even components refer to  $\tau$ -independent and  $\tau$ -dependent operators respectively. The spin-independent part  $v_{ij}^{SI}$  of the two-body potential is given by the first component  $v_{p=1}(r_{ij})$  only. The constants  $A_{p,m}$  and the functions  $F_m(r)$  are given in the appendix.

In the case of pure neutron matter (PNM), the isospin exchange operators are replaced by the identity.

We denote by  $v'_6$  the two-body potential model obtained by restricting the  $v'_8$  potential to the first 6 (3 for neutron matter) components. Note that this truncation of the Argonne  $v'_8$  should not be confused with the recently produced Argonne  $AV6'$  potential [30].

The three-body interaction used in our calculations of the equation of state is the Urbana IX potential [20]. For neutrons, the Urbana-IX interaction is given by the sum of a spin independent and a spin dependent part

$$V_{jkl} = V_{jkl}^{SI} + V_{jkl}^{SD} , \quad (7)$$

where

$$V_{jkl}^{SI} = U_0 \sum_{cyclic} T^2(m_\pi, c_3; r_{jl}) T^2(m_\pi, c_3; r_{lk}) ,$$

$$V_{jkl}^{SD} = B_{2\pi} \sum_{cyclic} \{X_{jl}^\pi, X_{lk}^\pi\} , \quad (8)$$

and the operator  $X_{jk}^\pi$  is given by

$$X_{jk}^\pi = Y(m_\pi, c_3; r_{jk}) \vec{\sigma}_j \cdot \vec{\sigma}_k + T(m_\pi, c_3; r_{jk}) S_{jk} . \quad (9)$$

The values of the parameters of the Urbana IX three-body potential, used in our calculations are shown in the appendix. Notice that in some of our earlier AFDMC calculations we have used  $c_3 = 2.0 \text{ fm}^{-2}$  and  $\mu = 0.7 \text{ fm}^{-1}$ , as given in the original papers proposing the Urbana IX potential [31] and the  $v'_8$  model interaction [12]. Changing  $c_3$  from 2.0 to 2.1 leads to a  $\sim 10\%$  additional increase of the three-body force contribution in neutron matter. In the following, we will denote with  $AU8'$  the  $v'_8$  plus Urbana IX interaction, with  $AU6'$  the  $v'_6$  plus Urbana IX interaction.

We have also considered the recently developed Illinois three-body potentials, which include two  $\Delta$  intermediate state diagrams [13], and denoted with IL1, ..., IL4.

### III. SPIN DEGREES OF FREEDOM

Standard Green's function or diffusion Monte Carlo methods for central potentials sample only the particle positions since the spin or isospin of the particles can be fixed. The Green's function Monte Carlo method used in light nuclei also samples the particle positions, but a complete description of the spin degrees of freedom is kept for each position sample leading to an exponential growth of the number of spin-isospin states with particle number  $A$ . This exponential behavior can be removed by sampling rather than summing the spin-isospin degrees of freedom.

We define a walker to be the  $3A$  coordinates of the  $A$  particles and  $A$  spinors each giving the four amplitudes for a particle to be in the proton up, proton down, neutron up and neutron down states. For the special case where walkers are sampled from the usual neutron-proton up-down basis, the spinors would be one of  $(1, 0, 0, 0)$ ,  $(0, 1, 0, 0)$ ,  $(0, 0, 1, 0)$ , and  $(0, 0, 0, 1)$  for each particle. Our auxiliary field method requires the more general definition as shown below.

As usual, the overlap of the walker bra with the trial ket is the wave function amplitude,

$$\langle R, S | \Psi_T \rangle \equiv \Psi_T(R, S) . \quad (10)$$

Direct sampling of the spin-isospin in the usual spin up/down basis requires a good trial function that can be evaluated efficiently. This can be most easily seen for the variational formalism, but the same analysis applies to Green's function or diffusion Monte Carlo. A variational Monte Carlo calculation can be formulated by minimizing the expectation value of the Hamiltonian,

$$\langle H \rangle = \frac{\langle \Psi_T | H | \Psi_T \rangle}{\langle \Psi_T | \Psi_T \rangle}$$

$$= \frac{\int dR \sum_{S,S'} \Psi_T^*(R, S') H_{S',S} \Psi_T(R, S)}{\int dR \sum_S |\Psi_T(R, S)|^2}, \quad (11)$$

where for a  $v_6$  interaction we would have

$$H_{S',S} = \langle S' | S \rangle \left[ -\frac{\hbar^2}{2m} \sum_n \nabla_n^2 \right] + \langle RS' | V | RS \rangle, \quad (12)$$

with a straightforward generalization for spin-orbit terms.

Variational Monte Carlo can be implemented with either spin sums [32, 33, 34]

$$\begin{aligned} \langle H \rangle &= \int dR E_L(R) P(R), \\ P(R) &= \frac{\sum_S |\Psi_T(R, S)|^2}{\int dR \sum_S |\Psi_T(R, S)|^2}, \\ E_L(R) &= \frac{\sum_{S,S'} \Psi_T^*(R, S') H_{S',S} \Psi_T(R, S)}{\sum_S |\Psi_T(R, S)|^2}, \end{aligned} \quad (13)$$

or spin samples [35]

$$\begin{aligned} \langle H \rangle &= \int dR \sum_S E_L(R, S) P(R, S), \\ P(R, S) &= \frac{|\Psi_T(R, S)|^2}{\int dR \sum_S |\Psi_T(R, S)|^2}, \\ E_L(R, S) &= \frac{\sum_{S'} \Psi_T^*(R, S') H_{S',S} \Psi_T(R, S)}{|\Psi_T(R, S)|^2}. \end{aligned} \quad (14)$$

In these equations,  $P$  is the probability density to be sampled and  $E_L$  is the local energy. A typical variational calculation would use the Metropolis algorithm to sample either  $R$  or  $R$  and  $S$  from  $P$ , and average the value of the local energy over these samples.

Notice that for an eigenstate of  $H$ , both  $E_L(R, S)$  and  $E_L(R)$  are constant. So, as for central potentials, the variance will be low if the trial function is accurate. Notice also that the spin sum  $S'$  in the definition of  $E_L(R, S)$  is polynomial rather than exponential in  $A$ . For example a pair potential will have only order  $A^2$  terms where two particles have different spin-isospin.

The variance per sample for complete spin sums will be lower than for spin samples. However, since the spin sums grow exponentially with particle number spin sampling should be more efficient for large particle number if the trial function can be evaluated efficiently for a single many-particle spin state  $S$ .

Unfortunately, all of the good trial wave functions currently used for large numbers of particles cannot be evaluated efficiently for a single many-particle spin state  $S$ . For example light nuclei variational Monte Carlo calculations are typically done using a pair product (or more complicated) wave function,

$$|\Psi_P\rangle = \mathcal{S} \prod_{j < k} f_{jk}^c \left[ 1 + \sum_p u_{jk}^p O_{jk}^p \right] |\Phi\rangle, \quad (15)$$

where  $\mathcal{S}$  symmetrizes the operator products, and  $|\Phi\rangle$  is the antisymmetric model state. While the symmetrizer produces all possible orderings of the operators and therefore gives  $\mathcal{O}(A^2!)$  terms, normally the commutator terms are fairly small and the ordering of the operators is sampled. However, even within a fixed ordering, each operator in the product term when operating on a single many-particle spin-isospin state will produce 4 or 8 new states depending on whether isospin exchange gives a new state.  $\mathcal{O}(A)$  operators out of the  $\mathcal{O}(A^2)$  total acting on a single state are enough to populate all the states. Therefore a straightforward evaluation of  $\langle RS|\Psi_P\rangle$ , for this wave function will have the same computational complexity as evaluating a complete set of spin-isospin states at the position  $R$ . Since computing all the states have the same cost as a single state, full spin sums are used for these calculations.

If good trial functions for spin-isospin dependent interactions can be devised which can be evaluated or sampled efficiently at a single many-particle space position and spin-isospin state, straightforward generalizations of standard central potential Monte Carlo methods, both variational and Green's function, with spin-state sampling will solve the nuclear many-particle Hamiltonian.

#### IV. THE AFDMC METHOD

Since direct evaluation of the pair product wave function is not computationally feasible for large numbers of particles, and so far we have no good methods of sampling these wave functions, we instead drop the operator terms altogether and sample the spin-isospin variables using a rather poor, but easy to evaluate, wave function. Since this wave function does not contain amplitudes of the spin states of the correct solution we cannot use it to sample the spins. Instead, we rewrite the propagator as an integral over auxiliary fields using the Hubbard-Stratonovich transformation

$$e^{-\frac{1}{2} \lambda O^2 \Delta t} = \frac{1}{\sqrt{2\pi}} \int_{-\infty}^{\infty} dx e^{-\frac{x^2}{2}} e^{x\sqrt{-\lambda \Delta t} O}, \quad (16)$$

where  $O$  can be a one-body operator. To make use of this transformation we write our propagator as the left-hand side of Eq. 16, so that the integrand of the right hand side is a product of one-body terms. The integrand has a form such that propagating a walker at  $|R, S\rangle$  results in another walker of the same form at  $|R', S'\rangle$ .

For  $N$  neutrons, the  $v_6$  two-body interaction can be split into two parts

$$\sum_{j < k} v_{jk} = B + \frac{1}{2} \sum_{j,\alpha,k,\beta} \sigma_{j,\alpha} A_{j,\alpha;k,\beta} \sigma_{k,\beta}, \quad (17)$$

where roman subscripts like  $j$  and  $k$  are particle labels while greek subscripts like  $\alpha$  and  $\beta$  are cartesian components. The matrix  $A$  and the scalar  $B$  are functions of

the particle positions,

$$\begin{aligned} B &= \sum_{j < k} [v_1(r_{jk}) + v_2(r_{jk})] , \\ A_{j,\alpha;k,\beta} &= (v_3(r_{jk}) + v_4(r_{jk}))\delta_{\alpha\beta} + \\ &\quad [v_5(r_{jk}) + v_6(r_{jk})][3\hat{r}_{jk} \cdot \hat{x}_\alpha \hat{r}_{jk} \cdot \hat{x}_\beta - \delta_{\alpha\beta}] . \end{aligned} \quad (18)$$

$A_{j,\alpha;k,\beta}$  is taken to be zero when  $j = k$ .  $A$  can be viewed as a  $3N$  by  $3N$  real symmetric matrix. It therefore has real eigenvalues and eigenvectors defined by

$$\sum_{k,\beta} A_{j,\alpha;k,\beta} \psi_n^{k\beta} = \lambda_n \psi_n^{j\alpha} . \quad (19)$$

The potential can be written as

$$\begin{aligned} \sum_{j < k} v_{jk} &= B + \frac{1}{2} \sum_{j,\alpha,k,\beta,n} \sigma_{j\alpha} \psi_n^{j\alpha} \lambda_n \sigma_{k\beta} \psi_n^{k\beta} \\ &= B + \frac{1}{2} \sum_{n=1}^{3A} (O_n)^2 \lambda_n , \end{aligned} \quad (20)$$

with

$$O_n = \sum_{j\alpha} \sigma_{j\alpha} \psi_n^{j\alpha} . \quad (21)$$

Each of the  $O_n$  is a sum of 1-body operators as required above.

After applying the Hubbard-Stratonovich transformation, the short time approximation for the propagator can be written as

$$\begin{aligned} \left( \frac{m}{2\pi\hbar^2\Delta t} \right)^{3A/2} \exp \left( -\frac{m|R - R'|^2}{2\hbar^2\Delta t} \right) e^{-B(R)\Delta\tau} \\ \prod_n \frac{1}{\sqrt{2\pi}} \int_{-\infty}^{\infty} dx_n e^{-\frac{x_n^2}{2}} e^{x_n \sqrt{-\lambda_n \Delta t} O_n} . \end{aligned} \quad (22)$$

The  $O_n$  do not commute, so we need to keep the time steps small so that the commutator terms can be ignored.

We sample a value of  $x$  for each of the  $3A$  auxiliary field variables. Once these values are known, the propagation reduces to a rotation in the spin space, and, therefore, to multiplying the current spinor value for each particle by the set of matrices given by the transformation above. For a given eigenvalue  $\lambda_n \leq 0$  in Eq.(20) the spin states of particle  $k$ ,  $|\eta'_k\rangle = a'_k |\uparrow\rangle + b'_k |\downarrow\rangle$  will be rotated to the new one  $|\eta_k\rangle$  having the following components

$$\begin{aligned} a_k &= a'_k (\cosh(\alpha_n) + \sinh(\alpha_n) \psi_n^z(k)) \\ &\quad + b'_k \sinh(\alpha_n) (\psi_n^x(k) - i \psi_n^y(k)) , \\ b_k &= b'_k (\cosh(\alpha_n) - \sinh(\alpha_n) \psi_n^z(k)) \\ &\quad + a'_k \sinh(\alpha_n) (\psi_n^x(k) + i \psi_n^y(k)) , \end{aligned} \quad (23)$$

where

$$\alpha_n = \Delta t |\lambda_n| x_n \sqrt{(\psi_n^x(k))^2 + (\psi_n^y(k))^2 + (\psi_n^z(k))^2} , \quad (24)$$

and  $x_n$  is the sampled Hubbard-Stratonovich value. For positive values of  $\lambda_n$ , one has a similar set of equations, in which  $\sinh(\alpha_n)$  is substituted with  $i \sin(-\alpha_n)$ .

Finally it is worth mentioning here that importance sampling has been used for the integral in the HS variables. The value of the overlap of the walker with the trial function will not be peaked around  $x_n = 0$ , but will be shifted. Rather than sampling from the gaussian we preferentially sample values where we predict the trial function will be larger. One way is to shift the sampled gaussian values with a drift term analogous to the drift term in diffusion Monte Carlo by replacing the  $\sigma$  operators by their expectation value at the current  $R, S$  value and taking the real part. That is we write

$$\begin{aligned} &\frac{1}{\sqrt{2\pi}} \int_{-\infty}^{\infty} dx_n e^{-\frac{x_n^2}{2}} e^{x_n \sqrt{-\lambda_n \Delta t} O_n} , \\ &= \frac{1}{\sqrt{2\pi}} \int_{-\infty}^{\infty} dx_n e^{-\frac{(x_n - \bar{x}_n)^2}{2}} e^{x_n \sqrt{-\lambda_n \Delta t} O_n} e^{\frac{-2\bar{x}_n x_n + \bar{x}_n^2}{2}} , \\ &\bar{x}_n = \text{Re} \left[ \sqrt{-\lambda_n \Delta t} \langle O_n \rangle \right] , \\ &\langle O_n \rangle = \frac{\langle \Psi_T | O_n | R, S \rangle}{\langle \Psi_T | R, S \rangle} , \end{aligned} \quad (25)$$

and sample the shifted gaussian, the last correction term is included in the weight. With this real shift and the compensating weight, only the efficiency of the algorithm is changed. We have tried other schemes using a discretized gaussian integration with altered probabilities and compensating weights with very little difference in the overall efficiency. In Ref. [36] a complex drift rather than the real drift in Eq. (25) has been used. Unlike our real drift above, this can change how the path constraint is applied.

### A. Three-body potential

For a neutron system the spin-dependent part of Urbana IX potential, given in eqs. (7) and (8) reduces to a sum of terms containing only two-body spin operators but with a form and strength that depends on the positions of three particles. As will be seen below, for a fixed position of the particles, the inclusion of three-body potentials of the Urbana IX type in the Hamiltonian does not add any additional complications. It simply changes the strength of the coefficients of the terms in the potential and can be trivially incorporated in the AFDMC calculations.

The anticommutator in Eq.(8) can be written as

$$\{X_{jl}^\pi, X_{lk}^\pi\} = 2 x_{jkl}^{\mu\nu} \sigma_j^\mu \sigma_k^\nu , \quad (26)$$

where

$$x_{jkl}^{\mu\nu} = y_{jl}y_{lk}\delta_{\mu\nu} + y_{jl}t_{lk}^{\mu\nu} + t_{jl}^{\mu\nu}y_{lk} + t_{jl}^{\mu\alpha}t_{lk}^{\alpha\nu}, \quad (27)$$

and

$$\begin{aligned} y_{jl} &= Y(m_\pi, c_3, r_{jl}) - T(m_\pi, c_3, r_{jl}), \\ t_{jl}^{\mu\nu} &= 3 T(m_\pi, c_3, r_{jl}) r_{jl}^\mu \hat{r}_{jl}^\nu. \end{aligned} \quad (28)$$

The spin-dependent part of the three-body interaction  $V_3^{SD}$  can then be easily incorporated in the matrix  $A_{j,\alpha,k,\beta}$  of Eq.(18), by the following substitution

$$A_{j,\alpha;k,\beta} \rightarrow A_{j,\alpha;k,\beta} + 2 \sum_l B_{2\pi} x_{jkl}^{\alpha\beta}. \quad (29)$$

Similarly the new terms in the Illinois potentials can be included into this matrix.

### B. The Spin-Orbit Propagator

A first order approximation [21] to the spin-orbit contribution to the propagator can be obtained by operating the derivative appearing in the  $\vec{L}_{jk} \cdot \vec{S}_{jk}$  operator on the free propagator  $G_0$

$$\begin{aligned} (\vec{\nabla}_j - \vec{\nabla}_k) G_0(R, R') = \\ -\frac{m}{\hbar^2 \Delta t} (\Delta \vec{r}_j - \Delta \vec{r}_k) G_0(R, R'), \end{aligned} \quad (30)$$

and substituting this expression back into the propagator. As a result, the spin-orbit part  $P_{LS}$  of the propagator is factored out and is finally written as

$$\begin{aligned} P_{LS} &= \exp \left( \sum_{j \neq k} \frac{m v_{LS}(r_{jk})}{4\hbar^2} [\vec{r}_{jk} \times (\Delta \vec{r})_{jk}] \cdot \vec{\sigma}_j \right) \\ &= \exp \left( \sum_{j \neq k} \frac{m v_{LS}(r_{jk})}{4\hbar^2} (\vec{\Sigma}_{jk} \times \vec{r}_{jk}) \cdot \Delta \vec{r}_j \right) \end{aligned} \quad (31)$$

where  $(\Delta \vec{r})_{jk} = \Delta \vec{r}_j - \Delta \vec{r}_k$  and  $\vec{\Sigma}_{jk} = \vec{\sigma}_j + \vec{\sigma}_k$ .

However a careful analysis of the above expressions show that they include some spurious contributions linear in  $\Delta t$ . In order to see this the wave function is expanded, as usual, in the integral form of the imaginary time Schrödinger equation keeping only linear terms

$$\begin{aligned} \Psi(R) &= \Delta t \left[ \frac{1}{2m} \sum_j \nabla_j^2 - V + E_0 \right] \Psi(R) \\ &+ \int dR' G_0(R, R') P_{LS} [\Psi(R)] \\ &- \sum_p \Delta \vec{r}_p \cdot \vec{\nabla}_p \Psi(R) + \dots \end{aligned} \quad (32)$$

At this point,  $P_{LS}$  is expanded by using the second form of this propagator given in Eq.(31) keeping both linear and quadratic terms in  $\Delta \vec{r}$ . The integral in  $R'$  can be done by taking into account that i) the gaussian integrates to one if there are no powers of  $\Delta \vec{r}$ ; ii) terms containing only one power of a  $\Delta \vec{r}$  integrate to zero; iii) quadratic terms containing powers of different components of  $\Delta R'$ , integrate to zero and iv) terms like  $(\Delta x'_j)^2$  integrate to  $\Delta t \hbar^2 / m$ .

We first consider the part coming from the linear terms in  $\Delta \vec{r}$  in both the wave function and  $P_{LS}$ . These terms, after integration give

$$- \Delta t \sum_{j \neq k} \frac{v_{LS}(r_{jk})}{4\hbar} [(\vec{\sigma}_j + \vec{\sigma}_k) \times \vec{r}_{jk}] \cdot \vec{\nabla}_j \Psi(R). \quad (33)$$

The expression above can be further simplified by interchanging the dummy indices  $j$  and  $k$

$$- \Delta t \sum_{j < k} v_{LS}(r_{jk}) [\vec{L} \cdot \vec{S}]_{jk} \Psi(R), \quad (34)$$

which is the spin-orbit contribution to the Hamiltonian multiplied by  $-\Delta t$ .

However the  $P_{LS}$  propagator includes other terms which are of the same order in  $\Delta t$ . They come from the quadratic  $\Delta \vec{r}$  terms of the expansion of  $P_{LS}$

$$\begin{aligned} \Delta t (V_2 + V_3) &= \Delta t \frac{m}{32} \sum_j \sum_{k \neq j} \sum_{p \neq j} v_{LS}(r_{jk}) v_{LS}(r_{jp}) \\ &(\vec{\Sigma}_{jk} \times \vec{r}_{jk}) \cdot (\vec{\Sigma}_{jp} \times \vec{r}_{jp}) \\ &= \Delta t \frac{m}{32\hbar^2} \sum_j \sum_{k \neq j} \sum_{p \neq j} v_{LS}(r_{jk}) v_{LS}(r_{jp}) \\ &\left\{ \vec{r}_{jk} \cdot \vec{r}_{jp} \vec{\Sigma}_{jk} \cdot \vec{\Sigma}_{jp} - \vec{\Sigma}_{jp} \cdot \vec{r}_{jk} \vec{\Sigma}_{jk} \cdot \vec{r}_{jp} \right\}. \end{aligned} \quad (35)$$

The terms with  $k = p$  give rise to a two-body additional effective potential  $V_2^{add} = -V_2$ ,

$$V_2^{add} = - \sum_{j < k} \frac{mr_{jk}^2 v_{LS}^2(r_{jk})}{8\hbar^2} [2 + \vec{\sigma}_j \cdot \vec{\sigma}_k - \vec{\sigma}_j \cdot \hat{r}_{jk} \vec{\sigma}_k \cdot \hat{r}_{jk}]. \quad (36)$$

The terms with  $k \neq p$  lead to a three-body additional effective potential  $V_3^{add} = -V_3$ , given by

$$\begin{aligned} V_3^{add} &= - \sum_{j < k < p} \text{cyclic} \frac{mr_{jk}r_{jp}v_{LS}(r_{jk})v_{LS}(r_{jp})}{16\hbar^2} \\ &\{ \hat{r}_{jk} \cdot \hat{r}_{jp} [2 + \vec{\sigma}_k \cdot \vec{\sigma}_j + \vec{\sigma}_p \cdot \vec{\sigma}_j + \vec{\sigma}_k \cdot \vec{\sigma}_p] \\ &- \vec{\sigma}_j \cdot \hat{r}_{jk} \vec{\sigma}_k \cdot \hat{r}_{jp} - \vec{\sigma}_p \cdot \hat{r}_{jk} \vec{\sigma}_j \cdot \hat{r}_{jp} \\ &- \vec{\sigma}_p \cdot \hat{r}_{jk} \vec{\sigma}_k \cdot \hat{r}_{jp} \}. \end{aligned} \quad (37)$$

Therefore in the actual propagation it is necessary to include explicitly these terms with opposite sign if one is using  $P_{LS}$  as given by Eq.(31).

An alternative method that we have also used comes from realizing that the counter terms are produced by the next order term in the series expansion of the exponential. These terms either average to zero, or are higher order in the time step or give incorrect contributions. Subtracting them gives the propagator,

$$\exp\left(\sum_{j \neq k} \frac{mv_{LS}(r_{jk})}{4i\hbar^2} [\vec{r}_{jk} \times (\Delta\vec{r})_{jk}] \cdot \vec{\sigma}_j\right) \\ \exp\left(-\frac{1}{2} \left[ \sum_{j \neq k} \frac{mv_{LS}(r_{jk})}{4i\hbar^2} [\vec{r}_{jk} \times (\Delta\vec{r})_{jk}] \cdot \vec{\sigma}_j \right]^2\right), \quad (38)$$

with the second exponential giving the required counter terms to include. The two forms are equivalent to first order in  $\Delta t$ .

### C. Trial wave function

In our calculations we use the simple trial function given by a Slater determinant of one-body space-spin orbitals multiplied by a central Jastrow correlation,

$$|\Psi_T\rangle = \left[ \prod_{j < k} f(r_{jk}) \right] \mathcal{A} \left[ \prod_j |\phi_j, s_j\rangle \right], \quad (39)$$

where  $\mathcal{A}$  is the antisymmetrizer of  $A$  particles. The overlap of a walker with this wave function is the determinant of the space-spin orbitals, evaluated at the walker position and spinor for each particle (for nuclear matter the spinor also includes the isospin), and multiplied by a central Jastrow product.

For unpolarized neutron matter in a box of side  $L$ , the orbitals are plane waves that fit in the box times up and down spinors. The usual closed shells are 2, 14, 38, 54, 66, 114, ... for neutrons and 4, 28, 76, ... for nucleons.

The Jastrow correlation function  $f(r)$  has been taken as the first component of the FHNC/SOC correlation operator  $\hat{F}_{ij}$ , which minimizes the energy per particle of either neutron or nuclear matter at the desired density [16] (see also Section V).

As noted in section III, a trial function with spin exchange and tensor correlations requires exponentially increasing computational work as the number of particles increases. The advantages of our trial function is that it is totally antisymmetric and for  $A$  particles requires order  $A^3$  operations to evaluate. However, it does not contain any amplitude generated by the tensor force where spins are flipped with a compensating orbital angular momentum. It is left to the AFDMC method to generate these missing components.

Other forms of a trial wave function can be used. For example including a linear combination of Slater determinants is possible as is modifying the orbitals to include spin correlations of backflow form [37]. Both of these avoid the exponential computational complexity, but may not capture the essential physics of the tensor force [38].

### D. Path Constraint

As in standard fermion diffusion Monte Carlo, the AFDMC method has a fermion sign problem. The overlap of our walkers with the trial function will be complex in general so the usual fermion sign problem becomes a phase problem.

To deal with this problem, we constrain the path of the walkers to regions where the real part of the overlap with our trial function is positive. We have also tried constraining the phase to that of the trial function as in the fixed phase approximation [39]. Both give about the same results, within error bars, and we report values where the real part is positive. For spin independent time reversal invariant potentials both reduce to the fixed-node approximation. It is straightforward to show that if the sign of the real part is that of the correct ground state, we will get the correct answer and small deviations give second order corrections to the energy. We have not been able to prove that this constraint always gives an upper bound to the ground state energy although it appears to do so for the calculations we have done to date. It seems likely that there is not an upper bound theorem for the mixed estimate of the energy. If forward walking or a path integral ground state technique [40, 41] is used, the method simply produces a better trial function and the energy must be an upper bound.

In the fixed node method [19] the nodal structure of the trial function is determined by the Slater Determinant. Similary, our path constraint is fully determined by the space spin Slater Determinant of Eq. (39). The Jastrow function therefore affects only the variance and not our final results.

### E. Tail corrections

Monte Carlo calculations are generally performed within the sphere of radius  $L/2$ , where  $L$  is the length of the box side. Usually tail corrections are estimated by integrating out the spin-independent part of the two-body potential from  $L/2$  up to infinity. We have made our calculations within the full simulation box, and, in order to include also the contribution from the neighbor cells, we have tabulated the Jastrow factor  $f(r)$  and the components  $v_p(r)$  of the two-body potential in the following form

$$\begin{aligned}
F(x, y, z) &= \prod_{mno} f(|(x + mL_x)\hat{x} \\
&\quad + (y + nL_y)\hat{y} + (z + oL_z)\hat{z}|) \\
V_p(x, y, z) &= \sum_{mno} v_p(|(x + mL_x)\hat{x} \\
&\quad + (y + nL_y)\hat{y} + (z + oL_z)\hat{z}|). \quad (40)
\end{aligned}$$

For the calculations shown, we found it adequate to include only the 26 additional neighbor cells corresponding to  $m$ ,  $n$ , and  $o$  taking the values  $-1$ ,  $0$ , and  $1$ .

Our results are therefore already tail corrected. We found that the standard way of treating tail corrections leads to results very close to ours, except when we consider model interactions which contain tensor forces, which are relatively long range forces.

The three body potential is not treated as the two body one. Here we have estimated the tail corrections to the three body potential from the PBFHNC variational results described in V. This analysis shows that such corrections are already very small for systems with 66 nucleons.

## F. The Algorithm

Finally, in this subsection we give the schematic structure of the AFDMC algorithm.

1. Sample  $|R, S\rangle$  initial walkers from  $|\langle\Psi_T|R, S\rangle|^2$  using Metropolis Monte Carlo.
2. Propagate the spatial degrees of freedom in the usual diffusion Monte Carlo way with a drifted gaussian for half a time step.
3. For each walker, diagonalize the potential matrix (two- and three-body terms).
4. Loop over the eigenvectors, sampling the corresponding Hubbard-Stratonovich variable and update the spinors for half a time step. Introduce approximate importance sampling of the Hubbard-Stratonovich variables, as discussed in the previous subsection.
5. Propagate the spin-orbit, using importance sampling.
6. Repeat 2, 3, and 4 in the opposite order to produce a reversible propagator to lower the time step error.
7. Combine all weight factors and evaluate the new value of  $\langle\Psi_T|R, S\rangle$ . If the real part is less than 0 include the walker in the evaluation of the mixed and the growth energies, and then enforce constrained path by dropping the walker. In general, the importance sampling makes the number of dropped walkers small.

8. Evaluate the averages of  $\langle\Psi_T|R, S\rangle$ , and  $\langle\Psi_T|H|R, S\rangle$  to calculate the mixed energy.
9. Repeat as necessary.

## V. FHNC AND PBFHNC CALCULATIONS

In this Section we present the method that we have used to estimate the finite size effects in AFDMC simulations. Such a method is made necessary by the fact that simulations with more than 100 nucleons are computationally very demanding. A many-body theory, like FHNC, based on integral equation techniques, in which the number of particles in the simulation box has no practical limitation seems to be the best candidate to do this.

FHNC theory was originally developed [42] to treat fermionic systems in the thermodynamic limit. However, FHNC has been recently reformulated to deal with a finite number of fermions in a periodic box, as those used for the Monte Carlo calculations [29]. Such a theory, denoted as Periodic Box FHNC (PBFHNC), is based upon the fundamental property of the FHNC cluster expansion to be valid at all  $1/A$  order [42, 43], and it has been developed for Jastrow-correlated wave functions. In the cases of a nucleonic system interacting via a central potential it has been shown that finite size effects are (i) not limited to the kinetic energy expectation value, and (ii) rather accurately estimated by PBFHNC calculations [25].

However, realistic correlations  $\hat{F}(ij)$  are spin-dependent and have an operatorial structure similar to that of the two-body potential, as in Eq.(2) (where the component  $p = 1$  corresponds to the Jastrow correlation). Therefore the PBFHNC developed in Ref. [29] cannot be used as such, but has to be generalized to treat spin-dependent correlations. The main problem is that the spin operators involved do not commute, namely  $[\hat{F}(ij), \hat{F}(ik)] \neq 0$ . This feature makes a full FHNC summation impossible and one has to resort to reasonable approximations for the spin-dependent correlations.

Such approximations are characterized by the fact that, whereas the cluster diagrams containing scalar correlations only are summed up with FHNC technique, only a limited set of cluster diagrams containing spin-dependent correlations are included in the calculation. The most tested and used approximation is the so called FHNC/SOC, described in Ref. [44]. In our calculations we have used the version adopted in [16] in order to compute the different correlation functions  $\hat{F}(i, j)$  at the various densities considered. We have considered only the three variational parameters corresponding to healing distance,  $d_c$ , of central ( $p = 1 - 4$ ) and spin-orbit correlations ( $p = 7, 8$ ), the healing distance,  $d_t$  of tensor correlations ( $p = 5, 6$ ), and the quencher,  $a_s$ , of the spin-isospin dependent correlation. The other variational parameters, like the spin-independent potential quencher and the correlation quenchers have been kept fixed at

TABLE I: Variational parameters used in our FHNC/SOC and PBFHNC calculations for the  $AU6'$  and  $AU8'$  potentials.  $r_0 = (3/(4\pi\rho))^{1/3}$  is the average distance between the neutrons.  $r_0$ ,  $d_c$  and  $d_t$  are given in fm. The reference density  $\rho_0 = 0.16 \text{ fm}^{-3}$  is the equilibrium density of nuclear matter.

$\rho/\rho_0$	$r_0$	$d_c(6)$	$d_t(6)$	$a_s(6)$	$d_c(8)$	$d_t(8)$	$a_s(8)$
0.75	1.258	1.761	4.695	0.9	2.264	4.528	0.8
1.00	1.143	1.714	4.571	0.9	2.285	4.571	0.8
1.25	1.061	1.485	4.752	0.9	2.228	3.960	0.8
2.0	0.907	1.723	4.595	0.8	2.267	4.535	0.7
2.5	0.842	1.768	4.715	0.8	2.189	5.004	0.7

TABLE II: FHNC/SOC energy per particle of neutron matter for the  $AU6'$  interaction, at various densities.  $T_F$  is the Fermi kinetic energy, and  $\langle T \rangle$  is the kinetic energy expectation value, corresponding to the average of the JF and PB kinetic energies.  $\langle V_2 \rangle$  and  $\langle V_3 \rangle$  are the expectation values of the two-body and three-body potentials respectively.  $\Delta E_2$  is the second order perturbative correction [45].  $\Delta E_{\text{elem}}$  is the contribution from the lowest order elementary diagram (see text). All the quantities, except  $\rho/\rho_0$ , are expressed in MeV.

$\rho/\rho_0$	$T_F$	$\langle T \rangle$	$\langle V_2 \rangle$	$\langle V_3 \rangle$	$E_{\text{FHNC}}$	$\Delta E_2$	$\Delta E_{\text{elem}}$
0.75	28.969	35.33	-22.67	2.58	15.2	-0.9	0.6
1.00	35.094	43.82	-28.58	5.17	20.4	-0.9	0.9
1.25	40.722	52.27	-34.11	8.53	26.7	-1.5	1.2
2.0	55.708	74.40	-46.93	27.29	54.8	-4.4	2.8
2.5	64.643	88.85	-53.36	44.72	80.2	-6.1	3.8

unity. The *optimal* values of such variational parameters for pure neutron matter are shown in Table I. They have been obtained by minimizing the average energy  $E_{av} = \frac{1}{2}(E_{JF} + E_{PB})$ , where the two energy expectation values  $E_{JF}$  and  $E_{PB}$  refer to the Jackson–Feenberg and Pandharipande–Bethe kinetic energy expressions respectively [44]. The usual constraint  $\frac{|E_{JF} - E_{PB}|}{E_{av}} \lesssim .005$  has been imposed in order to limit the range of variability of the free parameters in a region of reliability of the FHNC/SOC approximation. We have verified that in such region the normalization condition is fulfilled within a few percent.

The variational energies for the case of the  $AU6'$  interaction are reported on Table II. The Table also reports the second order CBF perturbative corrections  $\Delta E_2$  [45] and the contribution from the lowest order elementary diagram  $\Delta E_{\text{elem}}$ , as discussed in Ref. [25]. The not negligible value of  $\Delta E_{\text{elem}}$  indicates that the effect from elementary diagrams is larger than has been assumed in all the past FHNC/SOC calculations of the nuclear matter equation of state [25, 28]. In recent FHNC/SOC calculations of the equation of symmetric nuclear matter and pure neutron matter [18, 46] extra cluster diagrams with respect to the approximation used here have been included. Differences between the various FHNC/SOC calculations are within the predictive accuracy of the approximation.

In Table III we compare the results of two different

TABLE III: Comparison of the FHNC/SOC results for the  $AU8'$  interaction, obtained with correlation operator of the type  $f_6$  or of the type  $f_8$ . In the first case the contribution of the spin–orbit potential is calculated perturbatively from the  $AU6'$  Hamiltonian. For comparison, in the third column the results for the  $AU6'$  interaction are also reported. In all cases the contribution from elementary diagrams has been added.

$\rho/\rho_0$	$T_F$	$AU6'$	$AU8'(f_6)$	$AU8'(f_8)$
0.75	28.969	15.8	16.1	13.3
1.00	35.094	21.3	21.8	17.6
1.25	40.722	27.9	28.8	23.0
2.0	55.708	57.6	59.0	47.5
2.5	64.643	84.0	86.2	71.7

TABLE IV: Comparison of the energy  $E_2$  at the second order of the FHNC cluster expansion with the full FHNC energy,  $E_{\text{PBFHNC}}$ . The calculation has been performed for the  $v_6$  model interaction at  $\rho = 0.16 \text{ fm}^{-3}$  and Jastrow correlation factor.

$N$	$T_F$	$E_2$	$E_{\text{PBFHNC}}$
14	35.600	19.36	17.60
38	33.703	17.51	15.91
66	34.917	19.11	17.63
114	35.646	20.09	18.71
1030	35.139	19.46	18.04

FHNC/SOC calculations of the equation of state of neutron matter, carried out for the  $AU8'$  potential. In the first one ( $AU8'(f_6)$ ) the spin–orbit correlation is set equal to zero, whereas, in the second one ( $AU8'(f_8)$ ), is included. One can see that the introduction of the spin–orbit correlation leads to a large lowering in the energy. As it will be shown, we do not find such a lowering when the spin–orbit interaction is included in the AFDMC simulations. In the FHNC/SOC approximation the cluster contributions from spin–orbit correlations are correctly included only at the lowest order level. The many–body cluster contributions are essentially neglected. The large and attractive spin–orbit contribution found in the  $AU8'(f_8)$  calculation may be due to this inaccuracy. On the other hand it might be possible that nodal surface induced by the spin–orbit part of the interaction is not accurately described by our trial function.

In order to compute the finite size effects in a realistic way one should first generalize the PBFHNC theory to include SOC diagrams like in FHNC/SOC approximation. Work in this direction is in progress [47]. In this paper we limit ourselves to including only the two–body cluster diagrams for the two–body potential and the kinetic energy and the leading three–body cluster diagrams for the three–body potential [47] in the PBFHNC scheme. Such leading terms correspond to include up to two correlation operators in the three–body cluster diagrams. We will show that this approximation, hereafter denoted as PBFHNC/L, can already be used to roughly estimate the finite size effects.

TABLE V: PBFHNC/L results for the  $AU6'$  interaction at density  $\rho = 0.16 \text{ fm}^{-3}$ . The Fermi kinetic energy  $T_F$ , the expectation values of the kinetic energy  $\langle T \rangle$ , the two-body potential  $\langle V \rangle_2$  and the three-body potential  $\langle V \rangle_3$  are displayed together with the energy per particle  $E$  in MeV units.

$N$	$T_F$	$\langle T \rangle$	$\langle V \rangle_2$	$\langle V \rangle_3$	$E$
14	35.600	44.47	-29.41	4.31	19.37
38	33.703	42.41	-29.43	4.70	17.68
66	34.917	43.64	-29.07	4.82	19.39
114	35.646	44.40	-28.87	4.87	20.40
1030	35.139	43.88	-28.95	4.86	19.79

TABLE VI: As in Table V at density  $\rho = 0.32 \text{ fm}^{-3}$ .

$N$	$T_F$	$\langle T \rangle$	$\langle V \rangle_2$	$\langle V \rangle_3$	$\langle E \rangle$
14	56.512	74.33	-48.04	17.18	43.47
38	53.500	71.64	-50.25	19.36	40.75
66	55.428	73.41	-49.51	20.30	44.20
114	56.584	74.56	-48.94	20.78	46.40
1030	55.779	73.75	-49.08	20.84	45.51

The performance of the two-body cluster approximation to account for finite size effects is studied in Table IV. There, for a purely central potential without three-body force, PBFHNC/L and PBFHNC energies are compared at  $\rho = 0.16 \text{ fm}^{-3}$  for the range of particle numbers used in our quantum Monte Carlo simulations.

Tables V and VI give the PBFHNC/L results for the  $AU6'$  interaction at two different densities for a number of neutron systems. Notice that the energy differences between the cases with 66 and 114 neutrons are very close to those obtained in the AFDMC simulations, given in Tables VIII and IX. Systems with 14 and 38 neutrons are too small to be included in the finite size effects analysis.

## VI. RESULTS

### A. AFDMC results for neutron matter

Extensive neutron matter calculations have been carried out for the  $AU6'$  and  $AU8'$  interactions by considering 14, 38, 66 and 114 neutrons in a periodic box at various densities ranging from  $0.75\rho_0$  up to  $2.5\rho_0$ .

In figure 1 we show a typical behavior of the mixed and growth energy as a function the time step for 14 neutrons in a periodic box at  $\rho = 0.32 \text{ fm}^{-1}$  interacting via  $AU8'$ . At  $\Delta\tau = 5 \times 10^{-5} \text{ fm}^{-1}$  we have found that the statistical error are smaller than the extrapolation ones irrespective of the density and number of particles. All the calculations reported here have been obtained by using that value for the time step.

The 14 neutrons system is interesting because it is small enough to be studied by using other many body methods which become inefficient for larger systems. In order to provide a full set of results for this system in

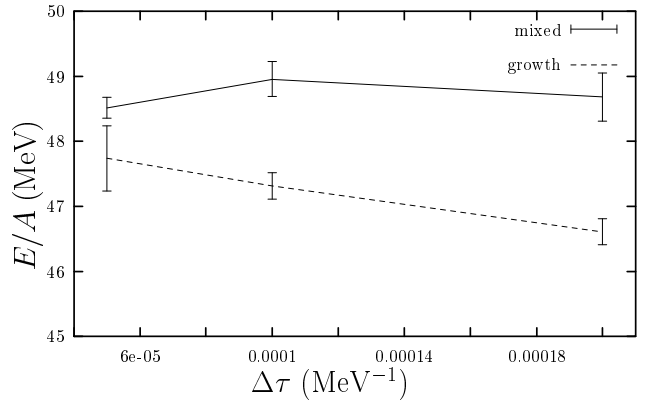


FIG. 1: Mixed and Growth energies versus the time step for 14 neutrons at  $\rho = 0.32 \text{ fm}^{-3}$  with the  $AU8'$  interaction.

TABLE VII: AFDMC energies per particle in MeV of 14 neutrons in a periodic box for interaction models at various densities. Error bars for the last digit are shown in parentheses.

$\rho(\text{fm}^{-3})$	$v'_6$	$v'_8$
0.12	12.41(4)	12.32(5)
0.16	15.12(4)	14.98(6)
0.20	17.86(5)	17.65(7)
0.32	27.84(6)	27.3(1)
0.40	36.0(1)	35.3(1)

table VII we report the energies at several densities calculated with the  $v'_6$  and  $v'_8$  interactions.

Diffusion Monte Carlo calculations using a pair-product wave function for 14 neutron systems have just been reported [28]. They however set the potential discontinuously to zero at distances greater than  $L/2$ , while we use either the nearest image convention or a lattice sum giving a continuous potential. We expect better extrapolation to large system sizes with the continuous potential as well as smaller time step errors. The time step errors will affect our AFDMC calculations more because we currently use the primitive approximation rather than building the Green's function from a product of exact two-body Green's functions. In principle we could use the Hubbard-Stratonovich breakup for the pair-product Green's function. In any case, we have carried out a calculation at  $\rho = 0.16 \text{ fm}^{-3}$  using the same discontinuous potential and obtained  $20.64(2)$  MeV and  $20.32(6)$  MeV for the  $v'_6$  and  $v'_8$  potentials respectively compared with their values of  $19.91(11)$  and  $17.00(27)$ . The larger difference when the spin-orbit term is included in the Hamiltonian may be due to the different trial wave functions used.

In Tables VIII and IX we report the results obtained with the AFDMC method of this work for neutron matter at the different densities considered for various system sizes. The extrapolation to infinite number of particles is carried out by using the PBFHNC/L results for a given

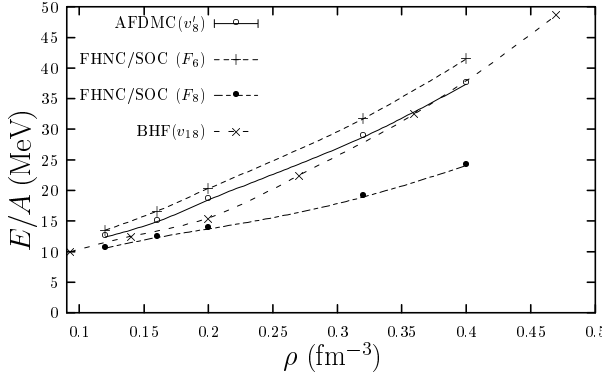


FIG. 2: AFDMC energy per particle for neutron matter with obtained from simulations with 66 neutrons and the  $v'_8$  potential. The variational FHNC/SOC results obtained with correlation functions of type  $F_6$  and  $F_8$  are and the Brueckner-Hartree-Fock (BHF) results of [48] also plotted and the The statistical error in the AFDMC results are smaller than the symbols.

number of neutrons and for the infinite system.

The spin-orbit contribution is rather small at all of the densities considered. This contrasts with previous FHNC/SOC calculations. In Fig. 2, we plot the AFDMC results together with the variational FHNC/SOC results for the  $v'_8$  interaction obtained by using correlation operators of the  $F_6$  and  $F_8$  forms, and the Brueckner-Hartree-Fock (BHF) results for the  $v_{18}$  potential [48]. One can see that SOC( $F_6$ ) and SOC( $F_8$ ) in the figure give quite different equations of state, particularly at high density. We have tried transient estimates and AFDMC simulations with orbitals of spin-backflow type for the 14 neutrons system finding not more than roughly 5% lowering of the energy [38].

The three-body potential gives a large contribution to the energy per particle at high densities. Therefore the search for a realistic three-body potential is a very fundamental problem for the study of dense and cold hadronic matter. A considerable amount of work has been done to find, in a semi-phenomenological way, three-body potentials to describe ordinary matter. However, whether such potentials are also valid in the high density regime is still an open and debated issue. In table X we report AFDMC results performed with the two body  $v'_6$  interaction and five different three-body potentials including the Urbana IX [12, 20] (UIX) and the recent Illinois 1 through 4 [13] three-body interactions. One can see that already at twice the nuclear matter density, the energy contributions from the three-body potentials are large and very different from each other, in spite of the fact that all of them provide a satisfactory fit to the ground state and the low energy spectrum of nuclei with  $A \leq 8$ .

In Fig. 3 we show the AFDMC equation of state for pure neutron matter with the  $AU8'$  interaction corresponding to the extrapolated values for infinite matter. We compare with the variational results of Akmal et al.

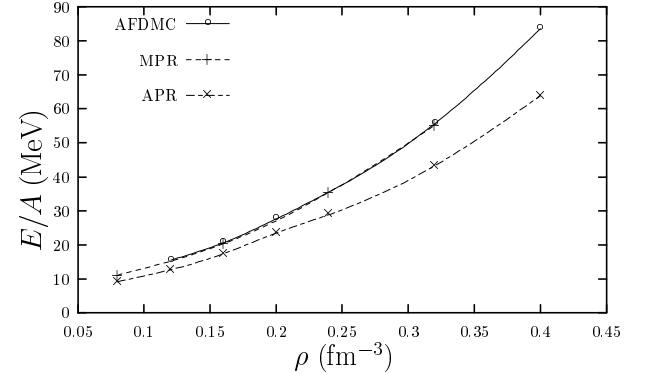


FIG. 3: Extrapolated AFDMC Equation of state of pure neutron matter with the  $AU8'$  potential (solid line). The variational results of Refs. [46] (APR, dotted-dashed line) and [18] (MPR, dashed line) corresponding to the Argonne  $v_{18}$  -two body plus Urbana IX -three body potential are also plotted. The lines are for guiding the eyes. The statistical errors of the AFDMC estimates are smaller than the symbols.

[46] and the more recent ones of Ref. [18] both of them obtained with the Argonne  $v_{18}$  2- and Urbana IX 3- nucleon interactions. One can see that there is a surprising good agreement between our AFDMC results and the latest variational calculation of Morales, Jr. et al. [18].

The compressibility  $\mathcal{K}$ , given by

$$\frac{1}{\mathcal{K}} = \rho^3 \frac{\partial^2 E_0(\rho)}{\partial \rho^2} + 2\rho^2 \frac{\partial E_0(\rho)}{\partial \rho}, \quad (41)$$

can be estimated from the equation of state by taking  $E_0 = E/A$ . For a Fermi gas the compressibility is  $\mathcal{K}_F = 9\pi^2 m/(k_f^5 \hbar^2)$ . The AFDMC results for  $\mathcal{K}/\mathcal{K}_F$  obtained from the extrapolated energies with  $AU8'$  are shown in Fig. 4. They are compared with the compressibility calculated from the variational energies of Ref. [18, 46].

## B. AFDMC results for nuclear matter

The AFDMC can deal with  $N \neq Z$  systems, and we have applied it to compute the asymmetry coefficient of the mass formula for the semirealistic two-body potential MS3 which is spin-isospin dependent but has no tensor force [49, 50]. The resulting values of  $E/A$  at  $\rho_0$  for symmetrical nuclear matter are given in Table XI, where they are also compared with the FHNC/SOC and PBFHNC results. The finite size correction is estimated from the corresponding PBFHNC results.

In Fig. 5 we plot the AFDMC energy per particle as a function of the asymmetry parameter,  $\alpha = (N - Z)/(N + Z)$ , of nuclear matter. The FHNC/SOC curve corresponds to a quadratic fit of nuclear matter ( $\alpha = 0$ ) and pure neutron matter ( $\alpha = 1$ ).

FHNC/SOC can only be used to study  $N = Z$  or  $N = A$  matter. The symmetry energy obtained from

TABLE VIII: AFDMC energies per particle in MeV for the  $AU6'$  interaction obtained with systems with 14, 38, 66 and 114 neutrons at various densities. Error bars for the last digit of the Monte Carlo calculations are shown in parentheses. The last column gives the extrapolated values from the PBFHNC/L calculation [47].

$\rho(\text{fm}^{-3})$	AFDMC(14)	AFDMC(38)	AFDMC(66)	AFDMC(114)	AFDMC( $\infty$ )
0.12	14.96(6)	13.76(9)	14.93(4)	15.62(8)	15.0
0.16	19.73(5)	18.56(8)	20.07(5)	20.99(9)	20.4
0.20	25.29(6)	24.4(1)	26.51(6)	27.6(1)	26.9
0.32	48.27(9)	49.8(1)	53.11(9)	55.3(2)	54.4
0.40	69.9(1)	74.5(2)	79.4(2)	82.2(2)	81.3

TABLE IX: AFDMC energies per particle in MeV for the  $AU8'$  interaction obtained with systems with 14, 38 and 66 neutrons at various densities. Error bars for the last digit of the Monte Carlo calculations are shown in parentheses. The last column gives the extrapolated values from the PBFHNC/L calculation [47].

$\rho(\text{fm}^{-3})$	AFDMC(14)	AFDMC(38)	AFDMC(66)	AFDMC( $\infty$ )
0.12	14.80(9)	13.96(5)	15.26(5)	15.5
0.16	19.76(6)	18.67(6)	20.23(9)	20.6
0.20	25.23(8)	24.7(1)	27.1(1)	27.6
0.32	48.4(1)	46.8(2)	54.4(6)	55.6
0.40	70.3(2)	76.3(2)	81.4(3)	83.5

TABLE X: AFDMC energies per particle in MeV for the  $v'_6 + \text{IL}$  potentials calculated with 66 particles. For the case of  $v'_6 + \text{IL2}$  interaction, at  $\rho = 0.32 \text{ fm}^{-3}$  the energies per particle with 38 and 54 neutrons are 12.6(2) and 10.0(3) MeV respectively.

$\rho(\text{fm}^{-3})$	$AU6'$	IL1	IL2	IL3	IL4
0.16	20.07(5)	11.2(1)	11.39(8)	12.0 (4)	10.5(2)
0.32	53.11(9)	8.0(4)	11.1(3)	14.7(3)	4.7(3)

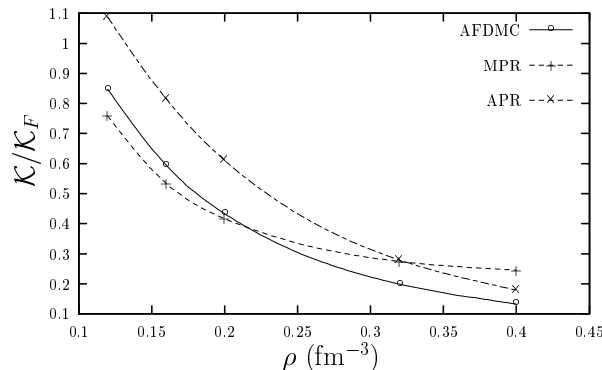


FIG. 4: Compressibility ratio,  $\mathcal{K}/\mathcal{K}_F$ , for neutron matter obtained from the extrapolated AFDMC energy per particle with the  $AU8'$  potential (solid line). The compressibility obtained from the variational results of Refs. [46] (APR, dotted-dashed line) and [18] (MPR, dashed line) is also plotted. The lines are for guiding the eyes. The statistical errors of the AFDMC estimates are smaller than the symbols.

FHNC/SOC is 41.59 MeV. The function  $E/A(\alpha)$  provided by the AFDMC results is not fully quadratic in  $\alpha$ , and corresponds to a symmetry energy of  $\sim 36.4$  MeV.

TABLE XI: Finite size corrections for symmetrical nuclear matter [25]: PBFHNC results for the MS3 potential at  $\rho = 0.16 \text{ fm}^{-3}$ . The PBFHNC calculations have been performed with a Jastrow correlated wave function, whereas the FHNC/SOC result has been obtained with a correlation operator of the type  $F_4$ . PBFHNC and FHNC/SOC calculations include the basic four-point elementary diagram  $E_4$ .

$A$	PB-FHNC	FHNC/SOC	AFDMC
28	-13.6	-	-16.17(6)
76	-15.6	-	-18.08(3)
2060	-14.0	-	$\downarrow$
$\infty$	-14.0	-14.9	-16.5(1)

## VII. OUTLOOK AND CONCLUSIONS

We have described a quantum Monte Carlo method specially suited to perform calculations on nucleon systems with noncentral interactions. It has been applied here to calculate the equation of state of pure neutron matter with fully realistic interactions by approximating it with up to 114 neutron in a simulation box. Finite size effects have been estimated by performing 2- plus 3- body cluster diagrams calculations based on PBFHNC method with spin-dependent correlations. The results obtained show an overall agreement with Brueckner-Hartree-Fock calculations and with a recent 2- plus 3- body cluster diagrams variational calculation [18]. They also indicate that there is a very small contribution coming from the spin-orbit component of the two-body interaction while the effect from the three-body potential is quite large, particularly at high densities. The large differences obtained for the equation of state for different phenomenological three-body potentials point out a three-body po-

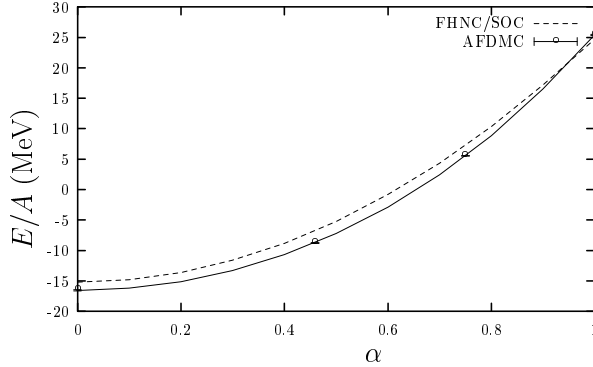


FIG. 5: AFDMC and FHNC/SOC energy per particle of nuclear matter for several values of the asymmetry parameter [25]. The lines correspond to polynomial fits of the calculated energies.

tential problem in the study of dense and cold hadronic matter.

Work in progress is to validate the present results using trial wave functions, other than the simple Slater determinant given in Eq. (39), that also can be calculated efficiently [38]. This will allow us to both lower the variance of our calculations, as is usual when better guiding functions are used in the importance sampling of the random walk, as well as to obtain a better path constraint.

We believe that our method should be able to produce accurate Monte Carlo calculations of a wide variety of nuclear systems. While previous Monte Carlo calculations have been severely restricted on the particle number by the spin-isospin sum this restriction is lifted by using the auxiliary field breakup of the spin-isospin part of the Hamiltonian, while using standard diffusion Monte Carlo for the spatial degrees of freedom. A pressing need is simulating nuclear matter with fully realistic interactions as already done for pure neutron matter; calculating the properties of light nuclei to compare with exact GFMC calculations; and investigating pion condensation. In addition, including explicit meson degrees of freedom can also be attempted. In the language of this paper, each meson field mode corresponds to an auxiliary field [22].

## Acknowledgments

We wish to thank A. Fabrocini, V. R. Pandharipande, A. Polls, S. Pieper, and R. Wiringa for helpful conversations. S. F. wish to thank the International Centre for Theoretical Physics in Trieste for partial support. A. S. acknowledges the Spanish Ministerio de Ciencia y Tecnología for partial support under contract BMF2002-00200

---

[1] V. R. Pandharipande, I. Sick, and P. K. A. deWitt Huberts, *Rev. Mod. Phys.* **69**, 981 (1997).

[2] G. G. Raffelt, *The stars as laboratories of fundamental physics* (University of Chicago, Chicago & London, 1996).

[3] R. F. Sawyer, *Phys. Rev. D* **11**, 2740 (1975).

[4] R. F. Sawyer, *Phys. Rev. C* **40**, 865 (1989).

[5] N. Iwamoto and C. J. Pethick, *Phys. Rev. D* **25**, 313 (1982).

[6] S. Reddy, M. Prakash, J. M. Lattimer, and J. A. Pons, *Phys. Rev. C* **59**, 2888 (1999).

[7] R. B. Wiringa, V. G. J. Stoks, and R. Schiavilla, *Phys. Rev. C* **51**, 38 (1995).

[8] V. G. J. Stoks, R. A. M. Klomp, C. P. F. Terheggen, and J. J. de Swart, *Phys. Rev. C* **49**, 2950 (1994).

[9] R. Machleidt, F. Sammarruca, and Y. Song, *Phys. Rev. C* **53**, R1483 (1996).

[10] V. G. J. Stoks, R. A. M. Klomp, M. C. M. Rentmeester, and J. J. de Swart, *Phys. Rev. C* **48**, 792 (1993).

[11] L. Engvik, M. Hjorth-Jensen, R. Machleidt, H. Müther, and A. Polls, *Nucl. Phys. A* **627**, 85 (1997).

[12] B. S. Pudliner, V. R. Pandharipande, J. Carlson, and R. B. Wiringa, *Phys. Rev. Lett.* **74**, 4396 (1995).

[13] S. C. Pieper, V. R. Pandharipande, R. B. Wiringa, and J. Carlson, *Phys. Rev. C* **64**, 14001 (2001).

[14] S. C. Pieper, K. Varga, and R. B. Wiringa, *Phys. Rev. C* **66**, 044310 (2002).

[15] A. Ramos, W. H. Dickhoff, and A. Polls, *Phys. Rev. C* **43**, 2239 (1991).

[16] R. B. Wiringa, V. Fiks, and A. Fabrocini, *Phys. Rev. C* **38**, 1010 (1988).

[17] A. Akmal and V. R. Pandharipande, *Phys. Rev. C* **56**, 2261 (1997).

[18] J. Morales, Jr., V. R. Pandharipande, and D. G. Ravenhall, *Phys. Rev. C* **66**, 054308 (2002).

[19] K. E. Schmidt and M. H. Kalos, in *Monte Carlo Methods in Statistical Physics*, edited by K. Binder (Springer-Verlag, Berlin, 1984), pp. 125–143.

[20] B. S. Pudliner, V. R. Pandharipande, J. Carlson, S. C. Pieper, and R. B. Wiringa, *Phys. Rev. C* **56**, 1720 (1997).

[21] S. C. Pieper, in *Microscopic Quantum Many-Body Theories and their applications. Lecture Notes in Physics*, edited by J. Navarro and A. Polls (Springer-Verlag, Berlin, 1998), vol. 510, p. 337.

[22] K. E. Schmidt and S. Fantoni, *Phys. Lett. B* **446**, 93 (1999).

[23] S. Zhang, J. Carlson, and J. E. Gubernatis, *Phys. Rev. Lett.* **74**, 3652 (1995).

[24] S. Zhang, J. Carlson, and J. E. Gubernatis, *Phys. Rev. B* **55**, 7464 (1997).

[25] S. Fantoni, A. Sarsa, and K. E. Schmidt, in *Advances in Quantum Many-Body Theory*, edited by R. F. Bishop, K. A. Gernoth, and N. R. Walet (World Scientific, Singapore, 2001), vol. 5, pp. 143–151.

[26] S. Fantoni, A. Sarsa, and K. E. Schmidt, *Prog. Part. Nucl. Phys.* **44**, 63 (2000).

[27] S. Fantoni, A. Sarsa, and K. E. Schmidt, *Phys. Rev. Lett.* **87**, 181101 (2001).

- [28] J. Carlson, J. Morales, Jr., V. R. Pandharipande, and D. G. Ravenhall (2003), nucl-the/0303041.
- [29] S. Fantoni and K. E. Schmidt, Nucl. Phys. A **690**, 456 (2001).
- [30] R. B. Wiringa and S. C. Pieper, Phys. Rev. Lett. **89**, 182501 (2003).
- [31] J. Carlson, V. R. Pandharipande, and R. B. Wiringa, Nucl. Phys. A **401**, 59 (1983).
- [32] J. Lomnitz-Alder, V. R. Pandharipande, and R. A. Smith, Nucl. Phys. A **361**, 399 (1981).
- [33] J. Carlson, Phys. Rev. C **38**, 1879 (1988).
- [34] E. Buendía, F. J. Gálvez, J. Praena, and A. Sarsa, J. Phys. G: Nucl. Part. Phys. **26**, 1795 (2000).
- [35] J. Carlson and M. H. Kalos, Phys. Rev. C **32**, 2105 (1985).
- [36] S. Zhang and H. Krakauer (2003), cond-mat/0208340.
- [37] S. Fantoni, in *Advances in quantum many body theories*, edited by A. Fabrocini, S. Fantoni, and E. Krotscheck (World Scientific, Singapore, 2002), vol. 7, pp. 379–405.
- [38] L. Brualla, S. A. Vitiello, A. Sarsa, S. Fantoni, and K. E. Schmidt, in preparation (2003).
- [39] G. Ortiz, D. M. Ceperley, and R. M. Martin, Phys. Rev. Lett. **71**, 2777 (1993).
- [40] S. Baroni and S. Moroni, Phys. Rev. Lett. **82**, 4745 (1999).
- [41] A. Sarsa, K. E. Schmidt, and W. R. Magro, J. Chem. Phys. **113**, 1366 (2000).
- [42] S. Fantoni and S. Rosati, Nuovo Cimento A **10**, 145 (1974); Lett. Nuovo Cimento **10**, 545 (1974); Nuovo Cimento A **25**, 593 (1975).
- [43] S. Fantoni and A. Fabrocini, in *Microscopic Quantum Many-Body Theories and their applications. Lecture Notes in Physics*, edited by J. Navarro and A. Polls (Springer-Verlag, Berlin, 1998), vol. 510, pp. 119–186.
- [44] V. R. Pandharipande and R. B. Wiringa, Rev. Mod. Phys. **51**, 821 (1979).
- [45] A. Fabrocini, private communication (2002).
- [46] A. Akmal, V. R. Pandharipande, and D. G. Ravenhall, Phys. Rev. C **58**, 1804 (1998).
- [47] F. Arias de Saavedra, A. Sarsa, S. Fantoni, and K. E. Schmidt, in preparation (2003).
- [48] M. Baldo, G. Giansiracusa, U. Lombardo, and H. Q. Song, Phys. Lett. B **473**, 1 (2000).
- [49] I. R. Afnan and Y. C. Tang, Phys. Rev. **175**, 1337 (1968).
- [50] R. Guardiola, in *Recent progress in Many-Body Theories. Lecture Notes in Physics*, edited by J. G. Zabolitzky, M. de Llano, M. Fortes, and J. W. Clark (Springer-Verlag, Berlin Heidelberg, 1981), vol. 142, pp. 398–406.

## APPENDIX A: POTENTIAL PARAMETERS

The  $A_{p,m}$  parameters in the expansion of the Argonne potentials, Eq. 6, are shown in Table XII.

The  $F_m$  functions in Eq. 6, are written as follows

$$\begin{aligned}
 F_1(r) &= T^2(\mu, c; r) , \\
 F_2(r) &= (1 + a_0 r) W(r) , \\
 F_3(r) &= \mu r W(r) , \\
 F_4(r) &= (\mu r)^2 W(r) , \\
 F_5(r) &= a_1 Y(m_0, c; r) - a_2 r W(r) , \\
 F_6(r) &= a_3 Y(m_c, c; r) - a_4 r W(r) , \\
 F_7(r) &= a_1 T(m_0, c; r) , \\
 F_8(r) &= a_3 T(m_c, c; r) ,
 \end{aligned} \tag{A1}$$

where the tensor, Yukawa and Wood–Saxon functions are defined as

$$\begin{aligned}
 T(m, c; r) &= (1 + \frac{3}{mr} + \frac{3}{(mr)^2}) \frac{e^{-mr}}{mr} (1 - e^{-cr^2})^2 , \\
 Y(m, c; r) &= \frac{e^{-mr}}{mr} (1 - e^{-cr^2}) , \\
 W(r) &= \frac{1}{1 + \exp(-5(r - 0.5))} .
 \end{aligned} \tag{A2}$$

The the coefficients  $a_0, \dots, a_4$  are shown in Table XIII and the masses  $m_0$ ,  $m_c$  and  $\mu$  and the cut-off parameter  $c$  are given in Table XIV.

The values of the parameters of the three-body Urbana IX potential are shown in table XV

TABLE XII: Argonne  $v8'$  two-body potential. Matrix  $A_{p,m}$  appearing in Eq.(6).

$p$	$A_{p,1}$	$A_{p,2}$	$A_{p,3}$	$A_{p,4}$	$A_{p,5}$	$A_{p,6}$	$A_{p,7}$	$A_{p,8}$
1	-7.52251741	2616.39024949	0	147.79390526	0	0	0	0
2	-0.12318501	84.20118403	0	-61.22868919	0	0	0	0
3	0.48726001	-82.48240972	0	49.26463509	0	0	0	0
4	0.65399916	-107.98800762	0	-20.40956306	1/3	2/3	0	0
5	0.94963459	-2.91931242	-424.28015518	-398.23289299	0	0	0	0
6	-0.17865545	-0.97310414	234.18526077	-256.12175941	0	0	1/3	2/3
7	-0.71193373	-373.43774331	0	653.08534247	0	0	0	0
8	-0.28568125	-201.79028547	0	354.25604242	0	0	0	0

TABLE XIII: Argonne  $v8'$  two-body potential. Values of the strength parameters in eqs. (A1) and(A2)

$a_0$ (fm $^{-1}$ )	$a_1$	$a_2$ (fm $^{-1}$ )	$a_3$	$a_4$ (fm $^{-1}$ )
0.37929090	3.15588245	10.48427302	3.48918764	11.21004425

TABLE XIV: Argonne  $v8'$  two-body potential. Values of the masses and cut-off parameters in eqs. (A1) and(A2)

$m_0$ (fm $^{-1}$ )	$m_c$ (fm $^{-1}$ )	$\mu$ (fm $^{-1}$ )	$c$ (fm $^{-2}$ )
0.68401113	0.70729025	0.69953054	2.1

TABLE XV: Urbana IX three-body potential. Values of the parameters appearing in Eq.(8).

$B_{2\pi}$ (MeV)	$U_0$ (MeV)	$m_\pi$ (fm $^{-1}$ )	$c_3$ (fm $^{-2}$ )
-0.0586	0.0048	0.69953054	2.1